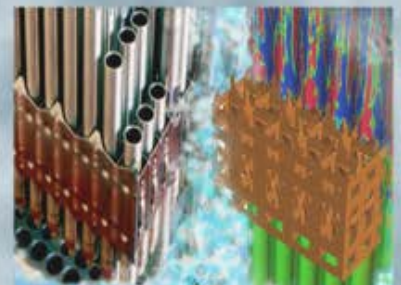
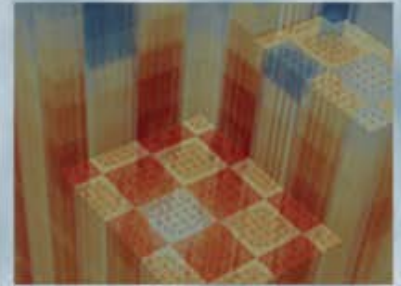


# Synthesis of CRUD and its Effects On Pool and Subcooled Flow Boiling

Carolyn Coyle, Jacopo Buongiorno,  
Thomas McKrell  
Massachusetts Institute of Technology,  
Cambridge, MA, USA

**March 31, 2015**



**Synthesis of CRUD and its Effects On Pool and Subcooled  
Flow Boiling**  
*CASL L3 Milestone Report*

Carolyn Coyle, Jacopo Buongiorno<sup>\*</sup>, Thomas McKrell  
Massachusetts Institute of Technology, Cambridge, MA, USA  
<sup>\*</sup>jacopo@mit.edu

## ABSTRACT

Previous studies have demonstrated the potential of porous, hydrophilic surfaces to lead to more efficient boiling. CRUD (Chalk River Unidentified Deposits) is a naturally occurring porous, hydrophilic layer that forms on fuel rods during reactor operation. Therefore, CRUD deposition can have large effects on critical heat flux (CHF) and heat transfer coefficient (HTC). An investigation of such effects is being conducted as part of this CASL project by preparing synthetic CRUD on indium tin oxide-sapphire heaters. These heaters are being tested in pool and flow boiling facilities in MIT's Reactor Hydraulics Laboratory. Synthetic CRUD was created using layer-by-layer deposition of 100 nm silica nanoparticles to form porous, hydrophilic thick films. Photolithography was used to manufacture posts that were then dissolved to create characteristic boiling chimneys. Features such as CRUD thickness, wettability, pore size, and chimney diameter and pitch were verified to be representative of reactor CRUD. Silica nanoparticles were used as a surrogate for reactor CRUD nanoparticle materials (iron and nickel oxides) since they create more stable films. To ensure accurate modeling, independent of material, 10 nm silica nanoparticle and 10 nm iron oxide nanoparticle boiling tests were conducted and compared. During testing, IR thermography and high-speed video are used to obtain two dimensional temperature profiles of the active heater area to quantify properties such as HTC, nucleation site density, and bubble departure frequency. Initial testing has demonstrated that heaters with synthetic CRUD (either silica or iron oxide-based) show roughly 100% enhancement in CHF and HTC over uncoated heaters. This report describes the synthetic CRUD fabrication process, while the full database for the boiling tests will be reported in the L2 Milestone Report due at the end of FY15.

**TABLE OF CONTENTS**

Abstract.....2

1. Introduction.....4

2. Background.....5

    2.1. CRUD Morphology.....5

    2.2. Boiling Heat Transfer and Surface Characteristics.....6

3. Experimental Methods.....7

    3.1. Manufacturing Synthetic CRUD.....8

    3.2. Synthetic CRUD Feature Verification.....10

    3.3. Apparatus and Procedure.....10

4. Results.....12

5. Conclusions and Future Work.....13

Nomenclature.....13

Appendix A: Machinery.....16

## 1. INTRODUCTION

CRUD, named for Chalk River Unidentified Deposits, is a layer of corrosion products that are transported by the reactor coolant, and deposit on fuel rods in nuclear reactor cores. Although CRUD effects on corrosion and reactivity have been studied extensively, its effects on reactor thermal-hydraulic performance have received less attention. Conducted research has been aimed primarily at understanding CRUD's composition, morphology, and deposition mechanisms, but CRUD's thermal properties and effects on fuel heat transfer and the boiling crisis are not well understood. Typically, CRUD buildup is thought to be a purely negative by-product of harsh nuclear environments that increases fuel's effective thermal resistance and temperatures. However, CRUD is a naturally occurring hydrophilic porous layer that, in surface characteristics studies, has been found to enhance CHF and increase the Leidenfrost temperature [1-4]. Therefore, in thin layers, CRUD has the potential to enhance heat transfer in the core during normal operation, postpone the boiling crisis in loss of flow accidents (LOFAs) or transient overpower, and accelerate quenching heat transfer following a loss of coolant accidents (LOCA) [5]. In order to fully understand these possible positive or negative consequences, models must be developed to simulate CRUD's effects on core thermal-hydraulics. Currently, programs such as the Consortium for Advanced Simulation of Light Water Reactors (CASL) have been working towards such a complete core model, with coupled neutronics, thermal hydraulics, and materials information that captures CRUD's evolution with operation [6]. This data could push the nuclear industry to not only model CRUD, but also control its thickness and morphology for optimized thermal performance throughout the irradiation cycle. Increased knowledge of CRUD is also important to the prediction of thermal margins, which relates to both reactor safety and economic performance. However, there is currently insufficient experimental information for accurate model validation.

**Table I. Reactor CRUD vs. synthetic CRUD morphology comparison.**

Properties	Reactor CRUD	Synthetic CRUD
Composition	Fe <sub>3</sub> O <sub>4</sub> , NiO, NiFe <sub>2</sub> O <sub>4</sub> , ZrO <sub>2</sub>	SiO <sub>2</sub>
Thickness	10-100 μm	5, 10, 15 μm
Roughness of Particle Region	R <sub>a</sub> ~0.5-3.0 μm	R <sub>a</sub> ~0.1-1.0 μm
Wettability (static contact angle)	10-30°	10-15°
Porosity	40-50%	40-60%
Pore Size	0.1-1 μm	~0.1 μm
Chimney Diameter	2-10 μm	5, 10 μm
Chimney Pitch	5-20 μm	10, 25, 100 μm

This CASL-sponsored work investigates the effects of CRUD buildup on the nucleate boiling heat transfer coefficient (HTC) and Critical Heat Flux (CHF). This objective is accomplished by creating well defined and characterized, synthetic CRUD with parameters representative of reactor CRUD, shown in Table I, and experimentally studying the effects of CRUD on the boiling heat transfer quantities of interest. Section 2 of this paper discusses the theory and background relevant to

this field. Section 3 covers CRUD synthesis and the proposed experimental procedure to study CRUD's effect on boiling heat transfer. Section 4 reports on the preliminary experimental results, while the conclusions are presented in Section 5.

## 2. BACKGROUND

It is important to study the characteristics of CRUD and mechanisms of boiling heat transfer to better understand how they relate.

### 2.1. CRUD Morphology

CRUD is a porous layer that collects on the surface of fuel rods during reactor operation. It is composed primarily of nickel oxide (NiO), iron oxide (Fe<sub>3</sub>O<sub>4</sub>), and trevorite (NiFe<sub>2</sub>O<sub>4</sub>), although relative quantities are unknown and depend greatly on individual reactor chemistry [5, 7]. These oxides are corrosion products of the reactor coolant system piping and components and are transported as particles throughout the reactor coolant system. As nucleate boiling occurs (either subcooled boiling in a PWR or saturated boiling in a BWR), the oxide particles precipitate onto the fuel pins [8]. CRUD can grow to 10-100 μm thick with average pore size, porosity, and roughness values between 0.1-1 μm, 40-50%, and 0.5-3.0 μm respectively [5]. CRUD also contains characteristic boiling chimneys, which are formed as water is pulled into the porous layer through capillary wicking, evaporates and escapes through the chimneys back into the coolant flow. Boiling chimneys are typically in the 2-10 μm range in diameter and have a 5-20 μm pitch. This morphology can be seen in Figure 1.

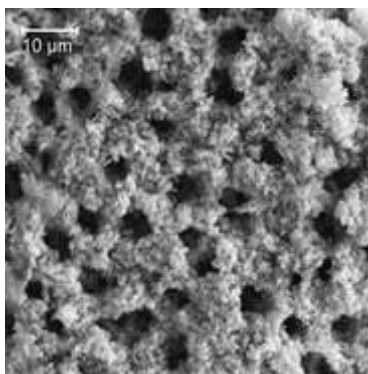


**Figure 1. CRUD from a PWR fuel assembly [9].**

Although corrosion products make up the majority of CRUD, species added to the reactor coolant, such as boron, also contribute to build up on fuel rods, leading to operational problems. Boron added to control reactivity can concentrate in the CRUD and change the neutron flux distribution in subcooled boiling regions, leading to CRUD induced power shifts (CIPS) [10]. Buildup of boric acid (H<sub>3</sub>BO<sub>3</sub>) and lithium hydroxide (LiOH) in thick CRUD can cause induced localized corrosion (ILC) of the zirconium cladding [5, 11]. However, this study will focus on CRUD deposition's effect on the thermal hydraulics and heat transfer of fuel rods and will neglect those phenomena. As a result, mechanisms of boiling heat transfer, specifically in porous media, must be well

defined.

## 2.2. Boiling Heat Transfer and Surface Characteristics

Boiling is a common mechanism of heat transfer in power generation systems. When discussing the efficiency of these systems, both CHF and heat transfer coefficient HTC should be considered. CHF designates the transition point from nucleate boiling to film boiling, while HTC describes a surface's ability to remove heat.

Zuber (1959) developed a well-accepted model to predict CHF based on hydrodynamic instabilities, shown in equation 1 [12],

$$q''_{CHF} = K \rho_g h_{fg} \left[ \frac{g \sigma (\rho_f - \rho_g)}{\rho_g^2} \right]^{1/4} \quad (1)$$

However, this model, like many others following it, fails to take into account the characteristics of the boiling surface. More recent and advanced models such as Kandlikar (2001), Polezhaev and Kovalez (1990), and Ramilison (1992) attempt to predict the pool boiling CHF accounting for factors such as wettability, porosity, and roughness [13–15]. Experimental studies have proven the importance of addressing surface effects [1–3]. O'Hanley (2013) demonstrated the ability of hydrophilic nano-porosity to increase CHF by 50-60% [3]. Similarly, the HTC is also affected by the introduction of surface features. Simple models of CRUD heat transfer consider only conduction through the layer and account for it as an additional thermal resistance [16]. More advanced 1D and 2D models such as those developed by Jones (1985), Henshaw (2006), and Haq (2011) account for contributions from fluid velocity and evaporation in the CRUD on heat removal and surface temperature [17-19].

When considering CHF and HTC without accounting for surface features, a larger number of fuel failures are expected than are observed in reactors [16]. This suggests an additional mechanism increasing the heat transfer efficiency of CRUD called wick boiling. In wick boiling, interconnected passages pull water into the hydrophilic, porous structure through capillary forces, opposed by viscous forces, and increase rewetting of the boiling surface, as shown in Figure 2 [16]. This increased coolant flow delays CHF. However, in a purely nano-porous, hydrophilic layer, the heat transfer from the surface is limited mainly by the vapor's ability to escape [20]. CRUD's formation of boiling chimneys naturally creates an outlet for vapor to quickly leave the porous structure and decrease the boiling surface temperature, increasing the HTC and delaying CHF. Equation 2 describes the 1D momentum flow of liquid through the CRUD porous structure and vapor escape through the chimneys [20].

$$4\sigma \left( \frac{1}{D_L} - \frac{1}{D_v} \right) = 32t \left[ \left( \frac{\mu V}{D^2} \right)_L + \left( \frac{\mu V}{D^2} \right)_v \right] + (\rho V^2)_L + (\rho V^2)_v \quad (2)$$

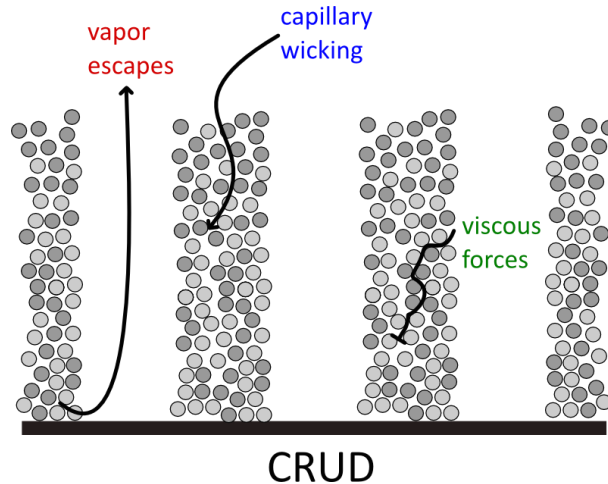


**Figure 2. Wick boiling diagram showing the locations of interest for capillary wicking, viscous forces and vapor escape.**

### 3. EXPERIMENTAL METHODS

Synthetic CRUD is created on specially designed wraparound, indium-tin oxide (ITO) sapphire heaters, as shown in Figure 3. The heaters are comprised of a 20 mm x 20 mm square, 1 mm thick sapphire base. Deposited on the base is an ITO layer that serves as a resistive heating element and is the active heating area where test data is gathered. CRUD is deposited on the ITO side of the heater and placed in contact with water. On the backside of the heater, two silver pads are printed on the ITO as connection points for electrodes. Having these connections on the backside removes them from contact with water, and prevents electrochemical corrosive reactions.

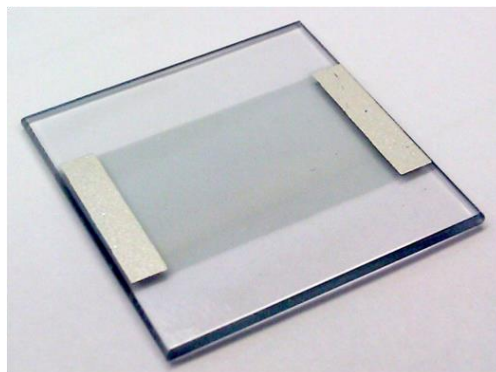


**Figure 3. ITO Sapphire Heater.**

#### 3.1. Manufacturing Synthetic CRUD

Synthetic CRUD is manufactured by creation of photoresist posts, layer-by-layer deposition of nanoparticles, and removal of posts. The detailed manufacturing process will be described here. Images of the machines used in this process can be found in Appendix A.

First, samples are plasma cleaned using oxygen plasma for 5 minutes under 500 mTorr to ensure the surface is clean and ready for fabrication. Next, photolithography is used to create post features that mark chimney locations from a photoresist polymer, such as SU-8 or AZ4620. Photoresist is deposited onto the heater surface using spin coating. By controlling the time and speed of the rotation, the thickness of the photoresist can be precisely controlled. Next, a mask with a two-dimensional chrome pattern of the desired features is placed in contact with the resist and exposed to UV light, transferring the pattern onto the resist. The heater is then placed in developing solution, removing undesired photoresist and leaving only the chosen pattern, as seen in Figure 4. By controlling the thickness of the photoresist and the size and spacing of the chrome features on the mask, post features can be made at any desired height, diameter, and pitch to model different chimney parameters.

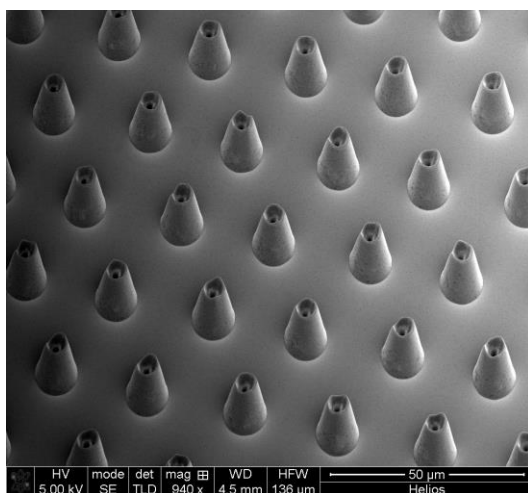


**Figure 4. 10  $\mu\text{m}$  Photoresist Posts on a 25  $\mu\text{m}$  Pitch.**

Once the photoresist posts have been made, charged 100 nm  $\text{SiO}_2$  nanoparticles are deposited onto the surface by layer-by-layer deposition. Particles are dipped in alternating positively charged PAH (polyallylamine hydrochloride) and negatively charged 100 nm  $\text{SiO}_2$  nanoparticle solutions as shown in Figure 5 [21]. Through electrostatic forces, this process builds a layer of  $\text{SiO}_2$  nanoparticles with consistent porosity of 50-60% and pore size on the order of particle size. The overall thickness of the layer is controlled by the number of dipping cycles.

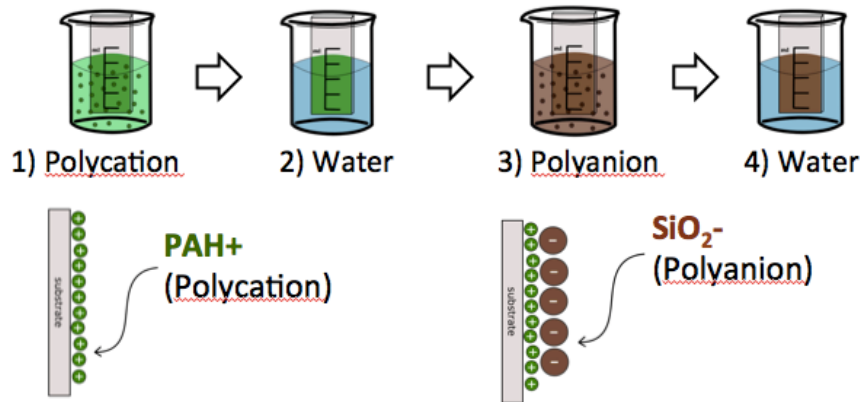


**Figure 5. Layer-by-Layer Deposition of 100 nm SiO<sub>2</sub> particles.**

After the layer-by-layer deposition process, the heaters are hydrothermally treated in an autoclave to enhance their mechanical durability. The heaters are placed in the autoclave and treated with saturated steam for 1 hour at 124°C [22]. Figure 6 shows high-resolution SEM images of the layer-by-layer surfaces before autoclaving and after 30 minutes and 1 hour of hydrothermal treatment. The hydrothermal treatment enhances the durability without greatly increasing particle necking and decreasing the porosity.

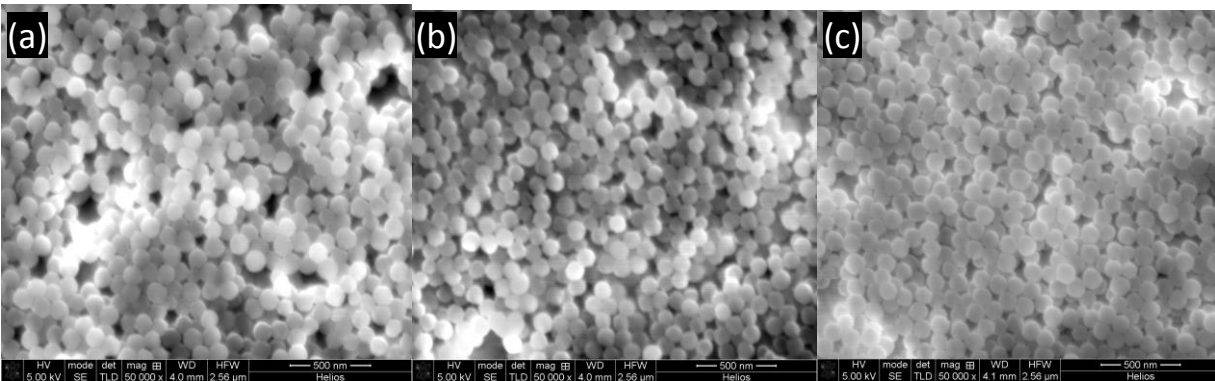


**Figure 6. SiO<sub>2</sub> surfaces (a) without treatment, (b) 30 min autoclaved, (c) 60 min autoclaved**

Finally, the posts are removed by boiling or acetone chemical dissolution to create chimneys on the heater surface.

By creating synthetic CRUD with this method, every aspect of the surface such as thickness, porosity, pore size, and chimney pitch and diameter can be precisely controlled. Although SiO<sub>2</sub> is not a component of reactor CRUD, there has been past success with its deposition in studies due to its stability and high surface charge [2, 3, 21]. Despite its different chemical makeup, the properties of SiO<sub>2</sub> suggest that it would be an acceptable alternative to manufacturing CRUD with Fe<sub>3</sub>O<sub>4</sub> or NiO, as shown in Table II. To ensure results will be representative of reactor CRUD, comparative 10 nm particle tests will be run with both SiO<sub>2</sub> and Fe<sub>3</sub>O<sub>4</sub> nanoparticles. Other properties such as wettability, porosity, and pore size will be kept constant.

**Table II. Material property comparison for particle selection [23-27].**

<b>Properties at 298 K</b>	<b>Fe<sub>3</sub>O<sub>4</sub></b>	<b>NiO</b>	<b>SiO<sub>2</sub></b>	<b>TiO<sub>2</sub></b>	<b>ZnO</b>
<b>Density (g/cm<sup>3</sup>)</b>	5.17	5.72	2.20	4.17	5.60
<b>Thermal cond. (W/mK)</b>	7.0	20.2	1.34	8.40	29.0
<b>Specific heat (J/kgK)</b>	0.62	0.53	0.74	0.71	0.50
<b>Thermal diffusivity (m<sup>2</sup>/s)</b>	$2.2 \times 10^{-6}$	$6.7 \times 10^{-6}$	$8.2 \times 10^{-7}$	$2.8 \times 10^{-6}$	$1.0 \times 10^{-5}$
<b>Surface energy (J/m<sup>2</sup>)</b>	0.79	2.4	1.0	1.29	1.31

From Table II, it is clear that the thermal conductivities of iron oxide and silica are different by a factor of 5. Therefore, the temperature of the wall in the case of silica nanoparticle CRUD will be higher than that of iron oxide CRUD of the same thickness and porosity. In order to have a consistent temperature increase across the CRUD layer, the ratio of thickness to thermal conductivity must be equivalent in both cases. Therefore, regarding wall temperature, the results of silica synthetic CRUD will be representative of the results of five times thicker iron oxide CRUD. This allows the experimental test matrix to explore a greater range of actual CRUD thickness without the same manufacturing constraints. With this particle substitute, it is also important to maintain the thickness to pore diameter ratio which is a significant dimensionless number for porous layers [3]. This follows a similar pattern to the CRUD thickness and with a five times thinner layer, the pore diameter must also be five times smaller. Because the pore diameter is roughly equal to the particle size, 100 nm silica particles are able to model the thermal behavior of 500 nm particles which is the middle of the reactor CRUD range. However, the ratio of capillary to viscous forces will still be representative of 100 nm pore sizes.

### **3.2. Synthetic CRUD Feature Verification**

Feature verification is an important part of the testing process and is used to ensure the integrity of the surface coating. These tests will be used to ensure that the synthetic CRUD maintains similar properties to real CRUD and that the data will be applicable to reactor environments.

The Dektak Profilometer in MIT's Microsystems Technology Laboratory (MTL) is used to measure the thickness and roughness of surface layers. The surface roughness  $R_a$ , or the average of the absolute values of feature heights, and linear roughness profiles are obtained. The static, advancing and receding contact angles of the liquid-solid-vapor interface of a droplet on the boiling surface are measured using the goniometer in MIT's Reactor Thermal Hydraulics Laboratory. These angles measure the wettability of the surface, i.e. whether the surface is hydrophilic or hydrophobic. A dual focused ion beam (FIB) and scanning electron microscope (SEM) in the MIT Center for Material Science and Engineering (CMSE) is used to gather images of the layer structure. The surface is bombarded with a FIB to cut into the layer and a SEM is used to visualize the cross section or capture surface images. Cross section and surface images are used to visualize CRUD formation and verify chimney size and location as well as porosity (void fraction). A representative image can be seen in Figure 7.

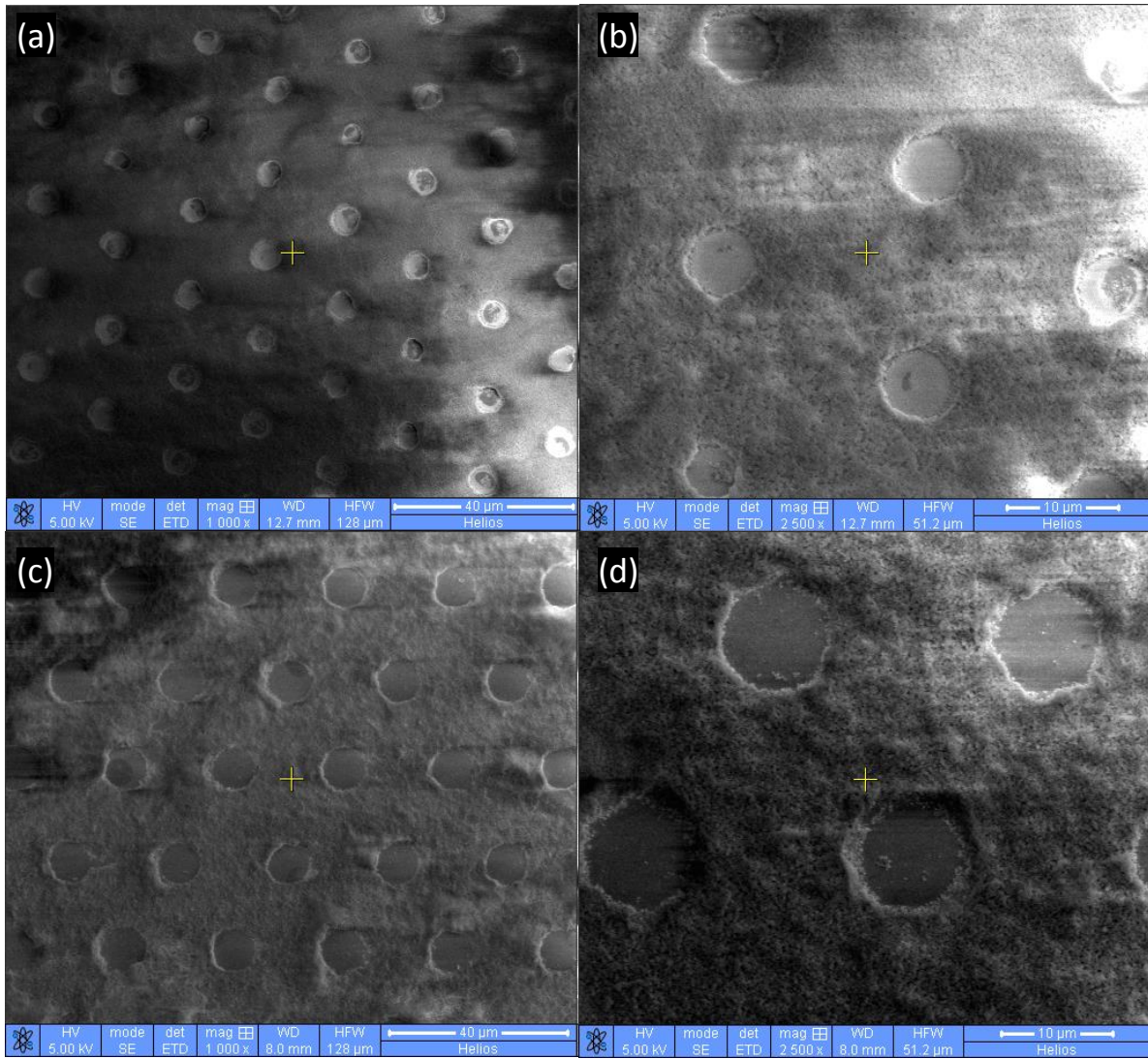


**Figure 7. Synthetic CRUD (a,b) 5  $\mu\text{m}$  chimney on 20  $\mu\text{m}$  pitch, thickness = 2  $\mu\text{m}$ ,  $R_a = 0.2 \mu\text{m}$ , static contact angle = 13°, (c,d) 10  $\mu\text{m}$  chimney on 25  $\mu\text{m}$  pitch, thickness = 1.5  $\mu\text{m}$ ,  $R_a = 0.15 \mu\text{m}$ , static contact angle = 15°.**

### 3.3. Apparatus and Procedure

The same flow boiling loop used in the CASL FY12-14 project will be used to test the boiling performance of the heaters with synthetic CRUD [28]. The loop consists of a pump, flow meter, preheater, heat exchanger, accumulator, a fill/drain tank, and various pressure and temperature sensors. The flow loop has a >1 m inlet section to attain fully developed flow that leads into a 220 mm tall, rectangular quartz test section. The quartz test section allows the flow to be imaged from all sides. Figure 8 shows the inlet and test sections and IR/HSV camera setup.

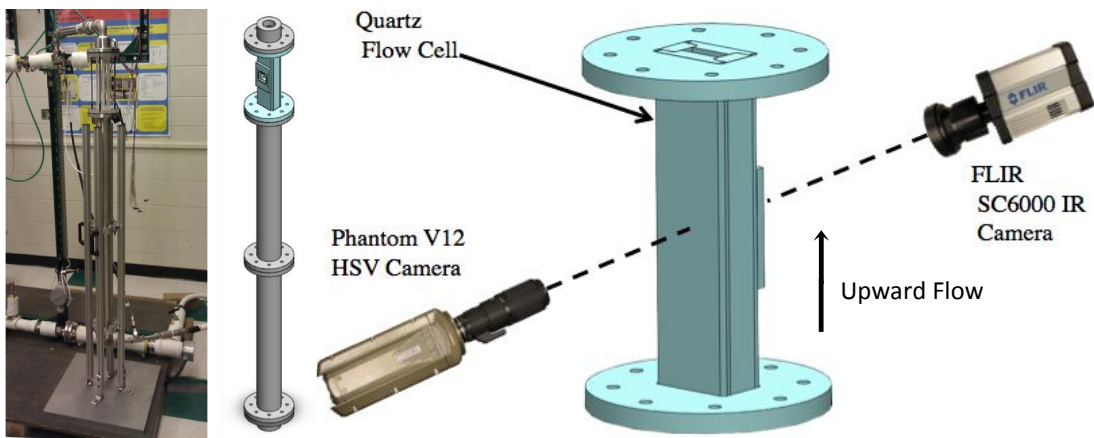


**Figure 8. Flow Boiling Loop and Schematic of Test Section and Camera Setup.**

Information about the various boiling parameters from the flow loop is gathered using both a FLIR SC6000 IR camera imaging the back side of the ITO and a Phantom V12 High Speed Video camera imaging from the boiling surface. The IR camera gathers a two-dimensional light intensity distribution which can be converted to the heater temperature distributions tuned through post-processing and calibration. Such distributions are then analyzed and used to calculate the average surface temperature and HTC as well as nucleation site density and bubble departure frequency information. An example of representative data is shown in Figure 9, taken by Phillips (2013) on bare heaters. The Phantom camera high-speed videos complement the IR images as well as monitor bubble sliding velocities.

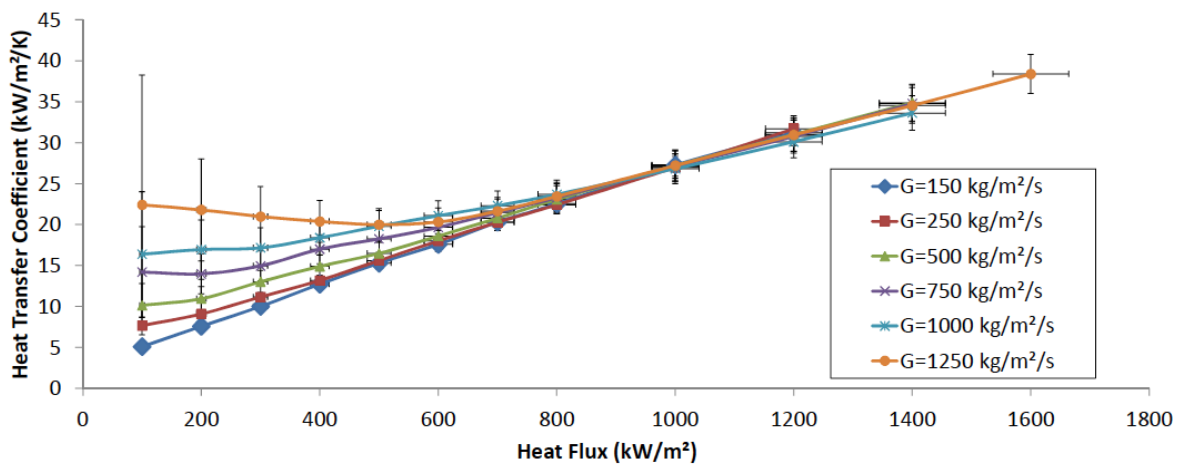


**Figure 9. Phillips (2013) HTC values for tests at 1.05 bar and 5°C subcooling [28].**

Table III shows the test matrix that will be used for this study where synthetic CRUD thickness and chimney pitch and diameter will be varied as well as the flow loop subcooling and mass flux.

This test matrix overlaps partially with the CASL FY12-14 tests, to ensure that a clean comparison between clean and CRUD-ed surfaces can be performed.

**Table III. Synthetic CRUD test matrix.**

Properties	Synthetic CRUD
Thickness	5, 10, 15 $\mu\text{m}$
Chimney Diameter	5, 10 $\mu\text{m}$
Chimney Pitch	10, 25, 100 $\mu\text{m}$
Subcooling	0, 5 $^{\circ}\text{C}$
Mass Flux	150, 250, 500, 750, 1000, 1250 $\text{kg}/\text{m}^2\text{s}$

At the present time initial screening tests of the heater surfaces have been conducted in a static (pool) boiling facility to ensure  $\text{SiO}_2$  nanoparticle surfaces are representative of  $\text{Fe}_3\text{O}_4$  surfaces. These tests are also meant to confirm surface durability, obtain preliminary results for CRUD's effects on HTC, and gather CHF data that could not be measured in the flow boiling loop.

Figure 10 shows the boiling curves and HTC curves for four surfaces: a bare heater, a  $\text{SiO}_2$  10 nm pore size, 1  $\mu\text{m}$  thick layer; an  $\text{Fe}_3\text{O}_4$  10 nm pore size, 1  $\mu\text{m}$  thick layer; and an  $\text{Fe}_3\text{O}_4$  10 nm pore size, 4  $\mu\text{m}$  thick with 10  $\mu\text{m}$  chimney diameter and 25  $\mu\text{m}$  chimney pitch CRUD layer. The final point of each curve represents heater failure. Uncertainties in heat flux results from Electronic Measurements Inc. TCR power supply with regulation and stability uncertainties of 0.1% and 0.05%.

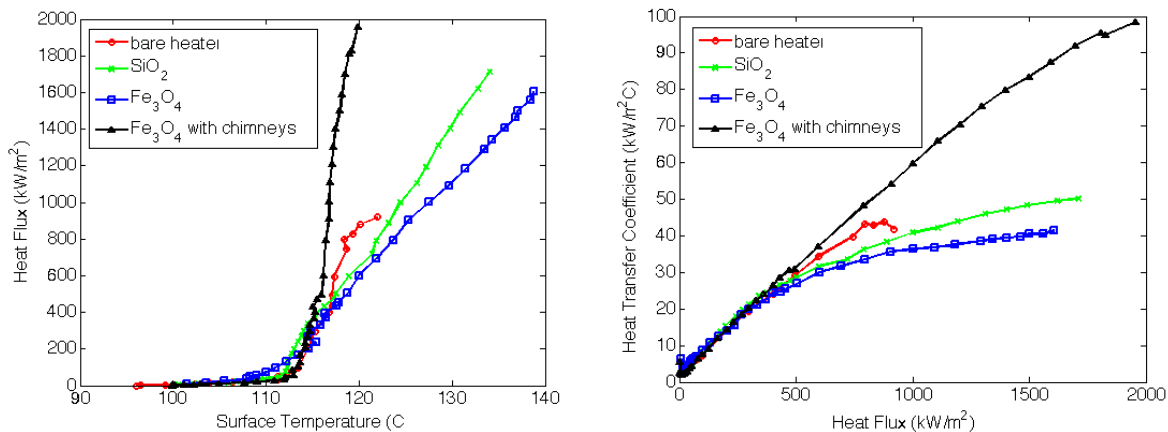


**Figure 10. Nanoparticle surface boiling and HTC curves for a bare heater, a 1  $\mu\text{m}$  thick 10 nm  $\text{SiO}_2$  layer, a 1  $\mu\text{m}$  thick 10 nm  $\text{Fe}_3\text{O}_4$  layer, and a 4  $\mu\text{m}$  thick 10 nm  $\text{Fe}_3\text{O}_4$  layer with 10  $\mu\text{m}$  chimney diameter and 25  $\mu\text{m}$  chimney pitch. Measurement uncertainties are roughly 1.15%.**

These preliminary pool boiling tests show that a thin layer of CRUD can enhance both CHF and HTC by roughly 100% over bare heaters. CHF and HTC values increase from 900  $\text{kW}/\text{m}^2$  to 2050  $\text{kW}/\text{m}^2$  and 40  $\text{kW}/\text{m}^2\text{C}$  to 100  $\text{kW}/\text{m}^2\text{C}$  respectively. This enhancement is very likely due to the wick boiling phenomena discussed above. The CRUD porous network allows greater rewetting

of the surface, increasing CHF, and the chimneys create locations for efficient vapor escape, increasing HTC. Figure 8 also shows that there is reasonably close agreement between the 10 nm SiO<sub>2</sub> particles and the 10 nm Fe<sub>3</sub>O<sub>4</sub> particles. The bare heaters have an average CHF value of 900 kW/m<sup>2</sup> where as the 10 nm SiO<sub>2</sub> and 10 nm Fe<sub>3</sub>O<sub>4</sub> heaters have CHF values of 1730 kW/m<sup>2</sup> and 1680 kW/m<sup>2</sup> respectively. The HTC values also agree to within 25%, which is a standard variation in such tests, even for heaters with the same coating. These HTC values, compared to uncoated heaters, also demonstrate the expected trends due to wick boiling. The porous layer increases rewetting due to capillary wicking and delays CHF; however, without chimneys, these surfaces do not display enhanced HTC over bare heaters.

#### 4. CONCLUSIONS AND FUTURE WORK

Initial testing demonstrates that the deposition of CRUD layers has the potential to significantly enhance CHF and HTC over clean surfaces. An Fe<sub>3</sub>O<sub>4</sub> 10 nm pore size, 4 μm thick with 10 μm chimney diameter and 25 μm chimney pitch CRUD layer enhanced CHF and HTC by roughly 100%. The above results also show that SiO<sub>2</sub> is a valid substitution for Fe<sub>3</sub>O<sub>4</sub> and that results obtained from silicon oxide will be representative of iron oxide results. Further testing varying both test conditions and CRUD surface features, as shown in Table III, will give insight into the individual effects of such parameters. Tests will be conducted in a flow boiling loop as shown in Figure 6 where the subcooling and mass flux can be changed. The composition of the synthetic CRUD will also be varied to determine how thickness and chimney pitch and diameter affect boiling parameters of interest such a nucleation site density and bubble departure frequency in addition to CHF and HTC. By studying the effects of CRUD and similar deposition layers, reactor heat transfer and boiling crisis can be better understood and predicted.

#### NOMENCLATURE

$h$	heat transfer coefficient	$D_v$	vapor chimney diameter
$q''_{CHF}$	critical heat flux	$D_L$	liquid capillary diameter
$K$	geometry coefficient	$t$	CRUD thickness
$h_{fg}$	latent heat of evaporation	$\mu_v$	vapor viscosity
$\rho_g$	vapor density	$\mu_L$	liquid viscosity
$\rho_f$	liquid density	$V_v$	vapor velocity
$\sigma$	surface tension	$V_L$	liquid velocity

#### REFERENCES

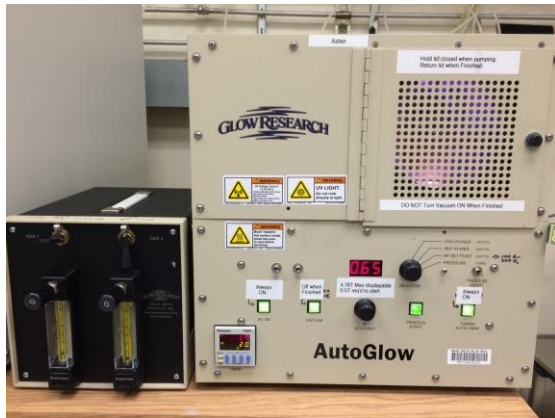
1. Kim, S.J., I.C. Bang, J. Buongiorno, and L.W. Hu. "Effects of Nanoparticle Deposition on Surface Wettability Influencing Boiling Heat Transfer in Nanofluids." *Applied Physics Letters* 89.15 (2006): 153107.
2. Forrest, E., et al., "Augmentation of Nucleate Boiling Heat Transfer and Critical Heat Flux Using Nanoparticle Thin-film Coatings." *International Journal of Heat and Mass Transfer* 53.1-3 (2010): 58-67.
3. O'Hanley, H., Coyle, C., Cohen, R., et al. "Separate Effects of Surface Roughness, Wettability,

- and Porosity on the Boiling Critical Heat Flux." *Applied Physics Letters* 103.2 (2013): 024102.
4. H. Kim, B. Truong, J. Buongiorno, L. W. Hu, "On the Effect of Surface Roughness, Wettability and Nano-Porosity on Leidenfrost Phenomena." *Applied Physics Letters*, 98 (2011): 083121.
  5. Buongiorno, J. "Can Corrosion and CRUD Actually Improve Safety Margins in LWRs?" *Annals of Nuclear Energy* 63(2014): 9-21.
  6. Yan, Jin, et al. "Multi-Physics Computational Models Development for Westinghouse PWRs." *Transactions of the American Nuclear Society* 109 (2013): 1643-45.
  7. La Fleur, B., D. Walter, and A. Manera. "Neutronic Effects of Nickel Ferrite CRUD without Boron Hideout." *Transactions of the American Nuclear Society* 109 (2013): 1295-298.
  8. Byers, W.A., "Pressurized Water Reactor Core Crud Mapping." *18th International Conference on Nuclear Engineering (ICONE 18)*, 2010. Xian China.
  9. Electric Power Research Institute (EPRI). "PWR Axial Offset Anomaly (AOA) Guidelines, Revision1." Technical Report (2003): 1003213.
  10. Deshon, J., D. Hussey, B. Kendrick, J. Mcgurk, J. Secker, and M. Short. "Pressurized Water Reactor Fuel Crud and Corrosion Modeling." *JOM* 63.8 (2011): 64-72.
  11. Short, M., D. Hussey, B. Kendrick, T. Besmann, C. Stanek, and S. Yip. "Multiphysics Modeling of Porous CRUD Deposits in Nuclear Reactors." *Journal of Nuclear Materials* 443.1-3 (2013): 579-87.
  12. N. E. Todreas, Mujid S. Kazimi, *Nuclear Systems I: Thermal Hydraulic Fundamentals*, Taylor & Francis 1993.
  13. Kandlikar, S.G. "A Theoretical Model to Predict Pool Boiling CHF Incorporating Effects of Contact Angle and Orientation." *Journal of Heat Transfer* 123.6 (2001): 1071.
  14. Polezhaev, Y.V., and Kovalev, S.A., "Modeling Heat Transfer With Boiling in Porous Structures." *Thermal Engineering* 37 (1990): 617-620.
  15. Ramilison, J.M., P. Sadasivan, and J.H. Lienhard. "Surface Factors Influencing Burnout on Flat Heaters." *Journal of Heat Transfer* 114.1 (1992): 287.
  16. Cinosi, N., I. Haq, M. Bluck, and S. Walker. "The Effective Thermal Conductivity of Crud and Heat Transfer from Crud-coated PWR Fuel." *Nuclear Engineering and Design* 241.3 (2011): 792-98.
  17. Pan, C., Jones, B.G., "Wick Boiling Performance in Porous Deposits with Chimneys," *AIChE/ANS National Heat Transfer Conference Symposium on Multiphase and Heat Transfer*. 1985.
  18. Henshaw, J., et al. "A Model of Chemistry and Thermal Hydraulics in PWR Fuel Crud Deposits." *Journal of Nuclear Materials* 353.1-2 (2006): 1-11.
  19. Haq, I., Nicolas Cinosi, Michael Bluck, Geoff Hewitt, and Simon Walker. "Modelling Heat Transfer and Dissolved Species Concentrations within PWR Crud." *Nuclear Engineering and Design* 241.1 (2011): 155-62.
  20. Macbeth, R.V., "Boiling on Surfaces Overlayed with a Porous Deposit: Heat Transfer Rates Obtained by Capillary Action." *Atomic Energy Establishment Winfrith AEEW-R-711*, 1971.
  21. Lee, D., M. Rubner, and R. Cohen. "All-Nanoparticle Thin-Film Coatings." *Nano Letters, American Chemical Society* 6.10 (2006): 2305-2312.
  22. Gemici, Z., Hiroomi Shimomura, Robert E. Cohen, and Michael F. Rubner, "Hydrothermal Treatment of Nanoparticle Thin Films for Enhanced Mechanical Durability." *Langmuir* 24.(2008): 2168-2177.

23. *CRC Handbook of Chemistry and Physics*, 95th Ed. 2014-2015
24. Beck, Michael. "Thermal Conductivity of Metal Oxide Nanofluids," Thesis. Georgia Institute of Technology, 2008.
25. Keem, J.E, and Honig, J.M., "Selected Electrical and Thermal Properties of Undoped Nickel Oxide". *CINDAS Report 52*, August 1978.
26. Leitner, Jindrich et al., "Estimation of Heat Capacities of Solid Mixed Oxides." *Thermochimica Acta*, 395. 1-2 (2002): 27-46.
27. Navrotsky, Alexandra. "Nanoscale Effects on Thermodynamics and Phase Equilibria in Oxide Systems." *ChemPhysChem*, 12.12 (2011):2207-215.
28. Phillips, B., J. Buongiorno, and T. McKrell, "Experimental Investigation of Subcooled Flow Boiling of Water at Atmospheric Pressure Using Synchronized High-Speed Video and Infrared Thermography." Paper 213, *The 15th International Topical Meeting on Nuclear Reactor Thermal Hydraulics*, NURETH-15, Pisa, Italy, May 12-15, 2013.

## APPENDIX A: MACHINERY

In order of use.



*Machine:* AutoGlow Plasma Cleaner

*Use:* Clean wafer before and after processing



*Machine:* Zeiss HMS Programmable Slide Stainer

*Use:* Layer-by-layer deposition of 100 nm SiO<sub>2</sub> nanoparticles



*Machine:* Solitec Spin Coater

*Use:* Coat heater surface with photoresist



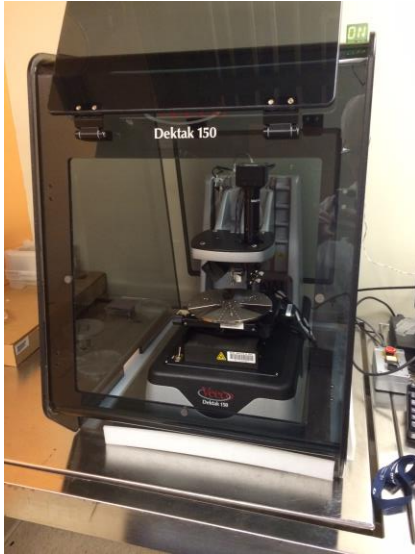
*Machine:* Tuttnauer-Brinkmann 2540E Autoclave

*Use:* Enhance mechanical durability



*Machine:* Karl Suss MA4 Aligner

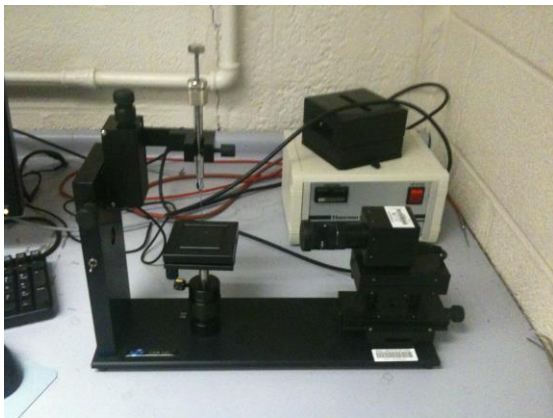
*Use:* Transfer mask pattern onto photoresist



*Machine:* Dektak 150 Profilometer  
*Use:* Measure thickness and roughness of surface



*Machine:* Helios Nanolab 600 Dual Beam Focused Ion Beam Milling System  
*Use:* Gain surface images and feature verification



*Machine:* KSV Instruments CAM 101 Goniometer  
*Use:* Contact angle measurements